Interplay between Kondo and magnetic interactions in $Pr_{0.75}Gd_{0.25}ScGeH$

Tyler Del Rose [a,b,*], Renu Choudhary [b], Yaroslav Mudryk [b], Daniel Haskel [c], Arjun K. Pathak [d], Gourab Bhaskar [e], Julia V. Zaikina [e], Duane D. Johnson [a,b], Vitalij K. Pecharsky [a,b]

[a] Department of Materials Science and Engineering, Iowa State University, Ames, IA 50011, USA
[b] Ames National Laboratory, US Department of Energy, Iowa State University, Ames, IA 50011, USA
[c] Advanced Photon Source, Argonne National Laboratory, Argonne, IL 60439, USA
[d] Department of Physics, SUNY Buffalo State University, Buffalo, New York 14222, USA
[e] Department of Chemistry, Iowa State University, Ames, IA 50011, USA

ARTICLE INFO

ABSTRACT

Combined experimental and density functional theory (DFT) study of $Pr_{0.75}Gd_{0.25}ScGe$ and its hydride ($Pr_{0.75}Gd_{0.25}ScGeH$) reveals intricacies of composition-structure-property relationships in those distinctly layered compounds. Hydrogenation of the intermetallic parent, crystalizing in a tetragonal CeScSi-type structure, leads to an anisotropic volume expansion, that is, $a(=b)$ lattice parameter decreases while the lattice expands along the c direction, yielding a net increase of cell volume. DFT calculations predict an antiparallel coupling of localized Gd and Pr magnetic moments in both materials at the ground state. While experiments corroborate this for the parent compound, there is no conclusive experimental proof for the hydride, where Pr moments do not order down to 3 K. DFT results also reveal that rare-earth – hydrogen interactions reduce spin-polarization of the Pr and Gd $5d$ and Sc $3d$ states at the Fermi energy, disrupt indirect exchange interactions mediated by conduction electrons, dramatically reduce the magnetic ordering temperature, and open a pseudo-gap in the majority-spin channel. Both experiments and theory show evidence of Kondo-like behavior in the hydride in the absence of an applied magnetic field, whereas increasing the field promotes magnetic ordering and suppresses Kondo-like behavior.

1. Introduction

Intermetallic RTX compounds and their hydrides, where R = rare-earth metal, T = transition metal, and X = *p*-block elements, attract considerable attention due to remarkable structural diversity and associated tunability of physical properties. Noteworthy are heavy-fermion, valence fluctuation, Kondo behavior, superconductivity, unusual topological effects, strong exchange bias, and complex sequences of magnetic structures [1–9]. Much of the fundamentally interesting physics in this family of materials emerges due to varying interactions between $4f$ and conduction electrons. Considering that the localized nature of $4f$ electrons prevents their direct overlap, conduction electrons mediate $4f$-$4f$ indirect exchange interactions, a mechanism known as Ruderman-Kittel-Kasuya-Yosida (RKKY) exchange [10–13]. Destabilization of the RKKY exchange through modified hybridization of $4f$ electrons with delocalized electron bands (usually *d* electrons) or disruption of conduction electron mediation at low temperatures, for example by warping of charge densities through additions of

electronegative species, can initiate heavy fermion, valence fluctuation, and/or Kondo behaviors.

From the original Kondo model, dilute $3d$ magnetic impurities (e.g., Mn impurities in a Cu matrix) enhance the scattering of conduction electrons in metals, resulting in increasing resistivity below a material-specific characteristic temperature [14]. Certain lanthanides, like Ce or Yb (less commonly, Pr, Sm, Eu, and/or Tm) can exhibit valence instabilities, fluctuating between non-magnetic Ce^{4+} ($4f^0$) or Yb^{2+} ($4f^{14}$) and magnetic Ce^{3+} ($4f^1$) or Yb^{3+} ($4f^{13}$) states, satisfying the dilute magnetic impurity prerequisite for Kondo interactions over a broad range of chemical compositions. Some of the best-known systems fitting this description are $Y_{1-x}Ce_x$ with $x \ll 1$ [15], where Kondo interactions with lanthanide impurities were first identified, and the Ag-Au-Yb system [16], which is perhaps the most well-studied Yb-containing Kondo system.

In addition to diluted Kondo systems, lanthanides form a few concentrated analogues (β-cerium is a prime example [17]), which, given their magnetic nature, are ideal systems to study the competition

---

Fig. 1. Crystal structures of (a) $Pr_{0.75}Gd_{0.25}ScGe$, (b) $Pr_{0.75}Gd_{0.25}ScGeH$ with hydrogen fully occupying the Ln_4 tetrahedra (red), and (c) $Pr_{0.75}Gd_{0.25}ScGeH_{1.5}$ with hydrogen fully occupying both the Ln_4 tetrahedra and the Sc_4Ln_2 octahedra (blue). Schematic in (a) illustrates the DFT unit cell used.

between Kondo and magnetic interactions. In this regard, RTX compounds, with appropriately selected R, and their hydrides ($RTXH_y$) are promising candidates to demonstrate this competition as the H-free parents exhibit diverse magnetism rooted in indirect RKKY interactions that may coexist with valence instabilities [9], [18], while hydrogen insertion may, as has been shown to, strongly influence both [19], [20]. For example, hydrogenation transforms a non-magnetic Kondo CeNiSn into a Kondo-antiferromagnet $CeNiSnH_{1.0}$ and then into a Kondo-ferromagnet $CeNiSnH_{1.8}$ [21]. Hydrogen insertion similarly transforms a non-magnetic Kondo CeRhSb into Kondo-antiferromagnetic $CeRhSbH_{0.2}$ [22].

In addition to Kondo interactions, hydrogenation of the CeScSi-type structure (Fig. 1) can lead to variable spin-polarization, electronic and magnetic disconnects between the lanthanide layers, and effective electronic-mass enhancements [23], [24]. In such systems, hydrogen commonly fills lanthanide $[Ln_4]$ tetrahedral interstices (red polyhedra in Fig. 1b-c), and, in some cases, $[Sc_4Ln_2]$ octahedral interstices (blue polyhedra in Fig. 1c), inducing unusual magnetic properties, [24,25]. For example, hydrogenation of GdTiGe [25], [26], NdScX [27], and CeScX [23] (with X = Si, Ge), dramatically reduces the magnetic ordering temperature and allows for the development of Kondo interactions. Likewise, a study of hydrogenated GdScGe notes a large reduction of Curie temperature (T_C), the development of a quasi-two-dimensional magnetic structure, and an unusual behavior of electrical resistivity [24].

Our recent study revealed that partial substitution of Gd for Pr in $Pr_{1-x}Gd_xScGe$ preserves the CeScSi-type structure regardless of x, leads to antiferromagnetic (AFM) coupling between Pr and Gd atoms, and permits several interesting magnetic features, such as strong exchange biases and magnetic memory effects [28], [29]. Here, we investigate hydrogenated $Pr_{0.75}Gd_{0.25}ScGe$ with emphasis on electronic behavior. We examine $Pr_{0.75}Gd_{0.25}ScGeH$ theoretically via DFT calculations and experimentally with X-ray diffraction and spectroscopy (X-ray magnetic circular dichroism and X-ray absorption near-edge structure), and physical property measurements to establish how the Gd-Pr substitution

and Gd/Pr-H interactions affect the overall physical properties of this system.

2. Material and methods

The polycrystalline $Pr_{0.75}Gd_{0.25}ScGe$ parent was prepared by arc-melting stoichiometric amounts of high-purity constituents: 99.3 wt% pure rare earths (with respect to all other elements) obtained from Ames Laboratory Materials Processing Center, and > 99.99 wt% pure Ge purchased from Meldford Metals. The alloy was annealed at 550 °C for one day, followed by three weeks at 950 °C, and subsequently slowly cooled back to room temperature. Further details can be found in Ref [28].

Hydrogenation was performed using PCTPro-2000 (Hy-Energy LLC) by placing samples into a stainless-steel autoclave under a 10 bar H_2 atmosphere at room temperature, followed by heating to 350 °C at a rate of 1 °C/min, holding for 12 h, and slowly cooling back to the ambient temperature at a minimum rate of 1 °C/min. For electrical resistivity measurements, several parallelepiped-shaped specimens of $Pr_{0.75}Gd_{0.25}ScGe$ were precut and hydrogenated, henceforth denoted *PCTPro* hydride. A few specimens broke during the hydrogenation process and were thus discarded. Additionally, the hydrogenated powder was consolidated into a pellet using Spark Plasma Sintering (SPS-211Lx, Sumitomo Coal Mining Co., Ltd) in a graphite die with inner diameter of 12.7 mm. The sintering was performed by heating of ~0.5 g of polycrystalline $Pr_{0.75}Gd_{0.25}ScGeH$ sample to 700 °C (at ~70 °C/min) under a uniaxial pressure of 103 MPa, holding for 10 min, cooling to 350 °C (at ~70 °C/min) followed by switching off the heater and releasing the pressure, all while a 97% Ar + 3% H_2 gas was flowed overtop. The resulting pellet was polished with sandpaper to remove residual graphite. The SPS consolidation resulted in an unquantified loss of hydrogen, forming a partially hydrogenated material, henceforth denoted *SPS* hydride. Neither of the materials shows signs of degradation when left in ambient conditions for extended periods.

Room-temperature powder X-ray diffraction (PXRD) measurements

Table 1

For $Pr_{0.75}Gd_{0.25}ScGe$ and its hydride: experimental and DFT lattice parameters and electronic specific heat (γ), DFT energy difference ($\Delta E = E_{FiM} - E_{FM}$) between ferrimagnetic (FiM) and ferromagnetic (FM) configurations of Pr/Gd, total number (spin-up + spin-down) of states at the Fermi energy ($n(E_F)$), and site-specific magnetic moments. Experimental lattice parameters of $Pr_{0.75}Gd_{0.25}ScGe$ are taken from Del Rose et al. [29].

Parameter	$Pr_{0.75}Gd_{0.25}ScGe$		$Pr_{0.75}Gd_{0.25}ScGeH$	
	Experiment	DFT	Experiment	DFT
$a(=b)$ (Å)	4.31578(2)	4.3212	4.25125(4)	4.2502
c (Å)	15.82624(6)	16.0274	16.8827(3)	16.8849
c/a	3.67	3.71	3.97	3.97
Cell volume (Å³)	294.779(3)	299.2759	305.123(8)	305.0122
Volume/atom (Å³/atom)	24.52	24.94	19.11	19.06
γ (mJ/mol K²)	8	9.35	28.7	13.22
$n(E_F)$ (states/eV f.u.)	3	3.96	12.2	5.61
ΔE (eV/atom)		-0.181		-0.087
DFT-Magnetic moment (μ_B/atom)	Pr1: $4f = -1.97$, $5d = -0.21$Pr2: $4f = -1.97$, $5d = -0.25$Gd: $4f = 6.96$, $5d = 0.04$Sc: 3d $= -0.243$		Pr1: $4f = -2.13$, $5d = -0.06$Pr2: $4f = -1.97$, $5d = -0.04$Gd: $4f = 6.95$, $5d = 0.143$Sc: 3d $= -0.03$	

were carried out at the 11-BM beamline of the Advanced Photon Source (APS) at Argonne National Laboratory (ANL) with $\lambda = 0.457897$ Å (more details in Del Rose et al. [29]) and on a modified TTRAX Rigaku system employing Mo Kα radiation [30]. Rietveld refinements were performed using the GSAS-II software [31]. Magnetic measurements were performed using a Quantum Design Inc. Superconducting Quantum Interference Device (SQUID) Magnetometer (MPMS XL-7). Electrical transport and heat capacity measurements were carried out in a Quantum Design Inc. Physical Property Measurement System (PPMS).

X-ray magnetic circular dichroism (XMCD) and X-ray absorption near-edge structure (XANES) measurements were carried out in a transmission geometry on powder samples at the 4-ID-D beamline (APS, ANL). Data were collected across the Gd L_2 (7.9303 keV) and L_3 (7.2428 keV), Pr L_2 (6.4404 keV) and L_3 (5.9643 keV), and Sc K (4.4928 keV) edges. For XMCD measurements, a superconducting magnet with a variable temperature insert was used to apply magnetic fields (± 20 kOe) collinear with the incident beam. Circularly polarized X-ray beams with opposite helicity were generated using a 180 μm-thick diamond phase plate [32]. All XANES and XMCD measurements were performed after cooling samples to the temperature of the measurement in zero field.

Density-functional theory (DFT) calculations were performed with plane waves using a projector augmented-wave (PAW) method, as implemented in the Vienna Ab-initio Simulation Package (VASP) [33], [34]. The generalized gradient approximation (GGA), as implemented by Perdew, Burke, and Ernzerhof (PBE), was used as the exchange-correlation function [35]. We also used an effective Hubbard U-J parameter of 5.3 eV for Pr and 6.0 eV for Gd to treat the strongly correlated $4f$ states. The experimentally determined lattice parameters of $a = b = 4.313$ Å and $c = 15.817$ Å for $Pr_{0.75}Gd_{0.25}ScGe$ and $a = b = 4.2527$ Å and $c = 16.9074$ Å for the hydride were used as inputs. The lanthanide site-disorder was modeled by lowering the symmetry to $P1$ and replacing one Pr atom in the unit cell with Gd, as illustrated in Fig. 1a. The convergence criterion for self-consistent calculations is 10^{-7} eV for the total energy per cell and an energy cutoff of 520 eV was used for the wavefunctions. The **k**-point integrations were performed using a tetrahedron method with Bloch corrections. A $16 \times 16 \times 4$ k-points (Γ-centered) grid was used for Brillouin-zone sampling.

3. Results and discussion

3.1. Crystal structure

$Pr_{0.75}Gd_{0.25}ScGe$ crystallizes in a tetragonal CeScSi-type structure (Fig. 1a without differentiation between Pr and Gd), which is a stacking of alternating corrugated lanthanide (Ln) layers and flat scandium sheets, with Ge separating the two. Previous reports on similar CeScSi-type structured hydrides show interstitial hydrogen can occupy the Ln_4 tetrahedra (Fig. 1b) [23,24,27,36] in addition to Sc_4Ln_2 octahedra (Fig. 1c) [24,27,36]. Locating H atoms in the hydrogenated $Pr_{0.75}Gd_{0.25}ScGe$ is complicated by the fact that neutron diffraction is practically impossible due to the exceedingly large neutron-absorption cross-section of the naturally occurring mixture of Gd isotopes. DFT results (see the Electronic-structure section for details), however, reveal that hydrogen energetically favors Ln_4 tetrahedra whereas Sc_4Ln_2 octahedra are unfavorable. Thus, we assume that H occupies only the Ln_4 interstices, hence, the fully hydrogenated compound is a mono-hydride $Pr_{0.75}Gd_{0.25}ScGeH$.

Full hydrogenation of $Pr_{0.75}Gd_{0.25}ScGe$ (*PCTPro* hydride) expands the c lattice parameter by 6.7% increasing the separation between the Sc sheets and the Ln layers, as well as between the Ln layers; these changes are likely to affect and weaken the interlayer magnetic interactions. At the same time, the $a(=b)$-axis contracts by 1.4%, resulting in slightly shorter Ln-Ln distances within the lanthanide layers, potentially enhancing the intra-layer Ln-Ln interactions. These peculiar competing features – more compact lanthanide layers and larger interlayer spacing – could result in a possible 2D magnetic behavior. The lattice constants of the *SPS* hydride ($a = b = 4.2668(5)$ Å and c $= 16.203(2)$ Å) are between those of the $Pr_{0.75}Gd_{0.25}ScGe$ parent and the fully hydrogenated (*PCTPro* hydride) material (listed in Table 1). Assuming the unit cell volume is a linear function of hydrogen concentration and that the *PCTPro* hydride is a monohydride, the estimated hydrogen content in the *SPS* hydride is 0.27 H/formula unit (f.u.).

Previously, reports describing GdScGe and GdScGeH [24,37] suggested that GdScGe may be slightly off-stoichiometric with ~1–2% of Gd occupying Sc (4c) sites, seemingly independent of x [29]. Therefore, a small, ~2% fraction of Gd atoms may also occupy the Sc site in $Pr_{0.75}Gd_{0.25}ScGeH$. This could lead to an interesting magnetic behavior where Gd atoms on the Sc site provide minor alterations to the long-range magnetic order.

To examine the effects of hydrogenation on the crystal structure further, an additional sample was synthesized following the same process outlined for the *PCTPro* hydride but under a 150 bar hydrogen pressure instead of the standard 10 bar, and powder X-ray diffraction (PXRD) data were collected at the 11-BM beamline (APS, ANL). All Bragg peaks can be indexed to the same CeScSi-type structure with little change in lattice constants when compared to the *PCTPro* hydride; however, many Bragg peaks with Miller indices $l >> h, k$ are broadened and can be interpreted as convolutions of peaks with varying widths, resulting in a poor Rietveld fit (Fig. S1, SI). Such peculiar peak shapes imply that hydrogenation lowers the crystallinity of $Pr_{0.75}Gd_{0.25}ScGe$. Worsening crystallinity after hydrogen absorption in these LnScGe materials is common [24]. We also considered a possibility of a hydrogen gradient from the surface to the core of individual particles, but the PXRD pattern can be fully indexed by a CeScSi-type structure with no peaks of non-hydrogenated $Pr_{0.75}Gd_{0.25}ScGe$, suggesting that the gradient, if any, is insignificant.

3.2. Physical properties

DC magnetic susceptibilities measured as functions of temperature for fully and partially hydrogenated materials are illustrated in Fig. 2. Magnetic susceptibilities of the fully (partially) hydrogenated samples measured in different magnetic fields, bifurcate below 40 (80) K, an indication of complex magnetic behavior. AC magnetic susceptibility
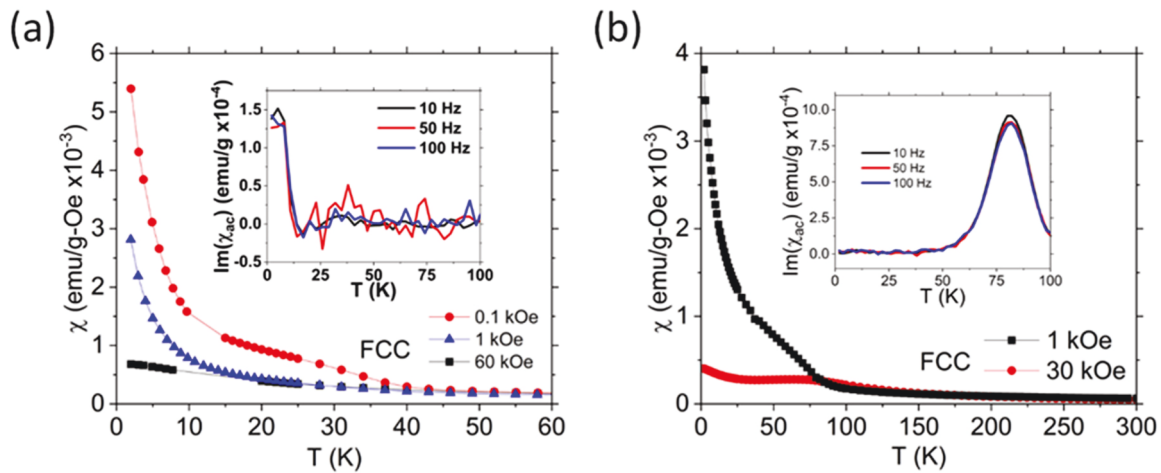
Fig. 2. DC Magnetic susceptibility as a function of temperature for (a) fully and (b) partially hydrogenated samples. Insets show the imaginary components of AC magnetic susceptibility for each sample.
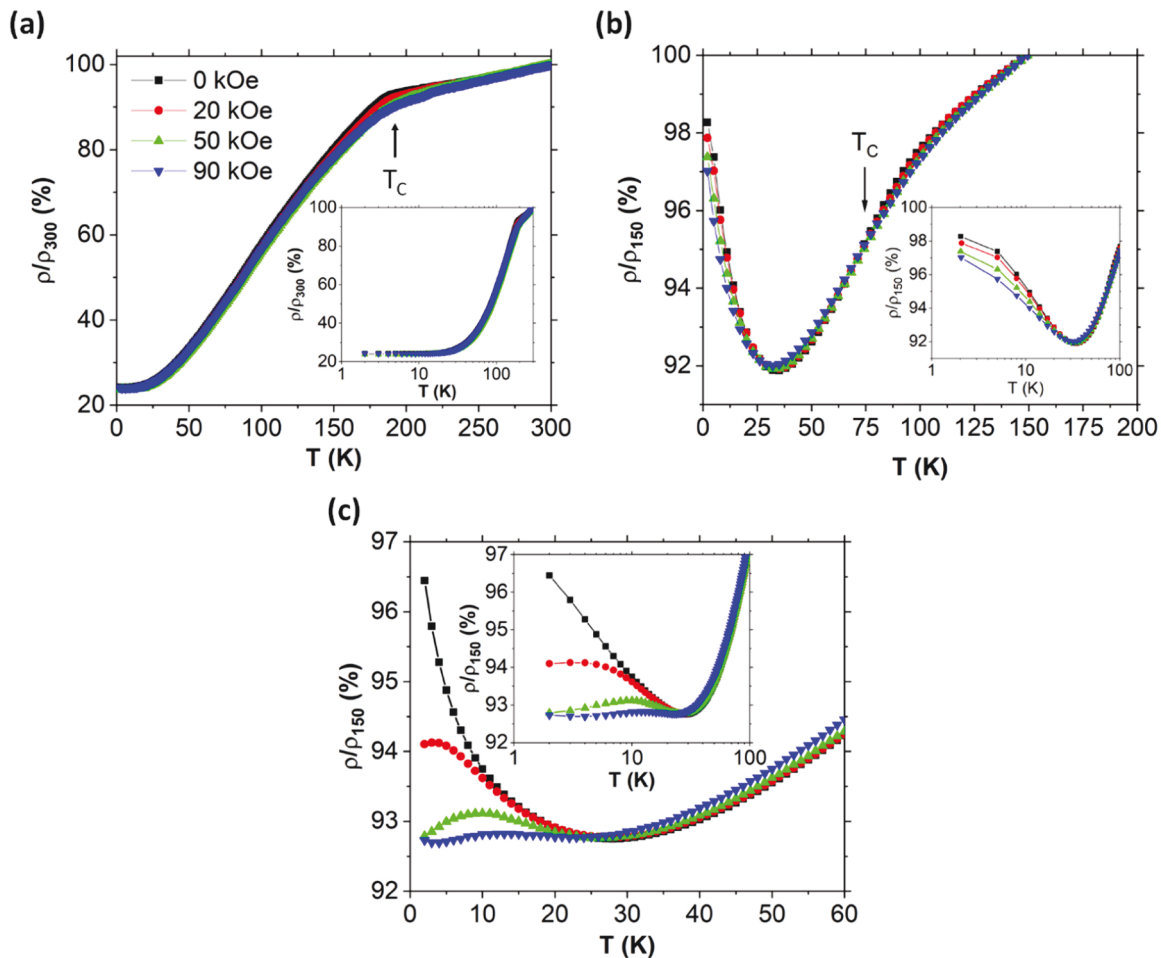

Fig. 3. Electrical resistivity measured as a function of temperature in varied magnetic fields for the (a) $Pr_{0.75}Gd_{0.25}ScGe$ parent, (b) *SPS* hydride, and (c) *PCTPro* hydride. Insets show electrical resistivities versus log(T).

measurements (insets in Fig. 2) show nearly frequency-independent energy losses at lower temperatures, 10 K and 70 K, respectively, which signal the formation of magnetic domains. Hence, the progressive insertion of hydrogen has a substantial effect on the ferrimagnetic long-range order, which in hydrogen-free $Pr_{0.75}Gd_{0.25}ScGe$ occurs at T_C = 190 K [28]. Note that a large difference between temperatures of the

anomalies seen in AC and DC measurements of the fully hydrogenated sample is peculiar in that domain formation usually implies the onset of long-range ferro- or ferrimagnetic ordering. Likewise, heat capacity measurements (Fig. S2, SI) do not have the usual λ-like anomaly indicative of a second-order transition (i.e., long range magnetic ordering). It is likely that the increased inter-Ln layer distances caused by hydrogen
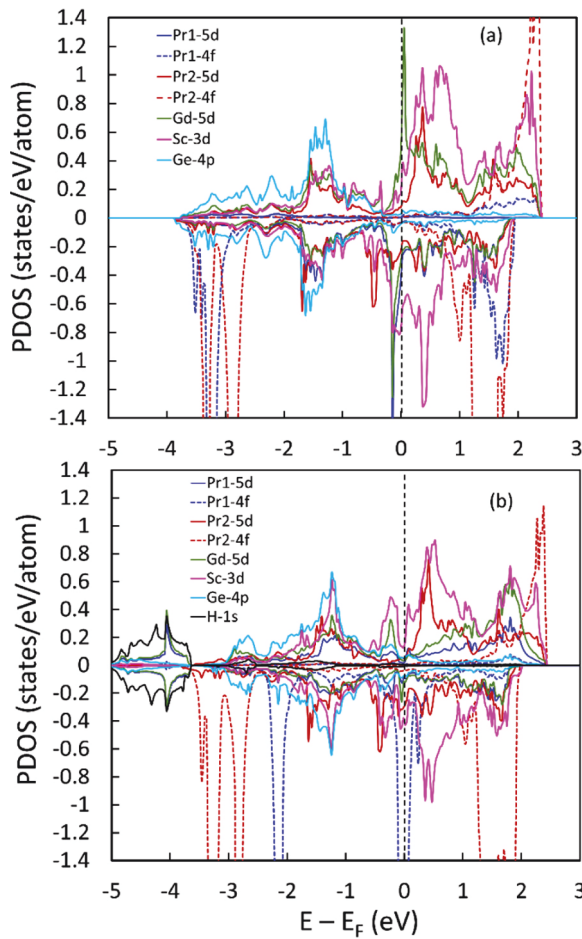
Fig. 4. Partial densities of states (PDOS) of (a) $Pr_{0.75}Gd_{0.25}ScGe$ and (b) $Pr_{0.75}Gd_{0.25}ScGeH$.

Fig. 5. Total density of states (TDOS) of (a) $Pr_{0.75}Gd_{0.25}ScGe$ and (b) $Pr_{0.75}Gd_{0.25}ScGeH$.

insertion have magnetically decoupled the Ln layers allowing for 2D or "quasi-2D" magnetic ordering to occur, as suggested for GdScGeH [24]. Experiments utilizing single crystals are needed to confirm this postulation.

Even though hydrogen intercalation increases the unit cell volume and, subsequently, the distances between the Ln layers, likely weakening RKKY exchange, the higher electronegativity of hydrogen is likely the main reason for a much-reduced T_C. As H is more electronegative compared to other elements present, the attraction of electrons to H alters the conduction electron density and disrupts the mediation of 4f-4f interactions. Furthermore, 4f-states of Pr can be located close to the Fermi energy [38], allowing for a modified 4f-5d (and 6s) hybridization, decreasing 4f localization, and thus also weakening the RKKY exchange.

The zero-field electrical resistivity (ρ) shows obvious changes in the signs of dρ(T)/dT from positive (metallic) to negative (Kondo-like) at low-temperatures in both hydrogenated $Pr_{0.75}Gd_{0.25}ScGe$ specimens. True Kondo behavior is also characterized by the linearity of electrical resistivity as a function of log(T), seen in zero-field data in the insets of Fig. 3b (roughly linear) and 3c (linear). Even though the *SPS* hydride (Fig. 3b) retains positive to negative sign changes in dρ(T)/dT at low temperature and fields up to 90 kOe, it does not constitute a Kondo system as the material is magnetically-ordered below 70 K (Fig. 2b), well above the temperature at which "Kondo-like" resistivity becomes distinguishable, in contradiction to Kondo theory [14]. Similarly, for the *PCTPro* hydride, the prominently increasing deviations from linearity as magnetic field increases (Fig. 3c) indicate suppression of Kondo-like scattering bringing into question whether this behavior can be explained with Kondo theory. The dρ(T)/dT sign changes in a high

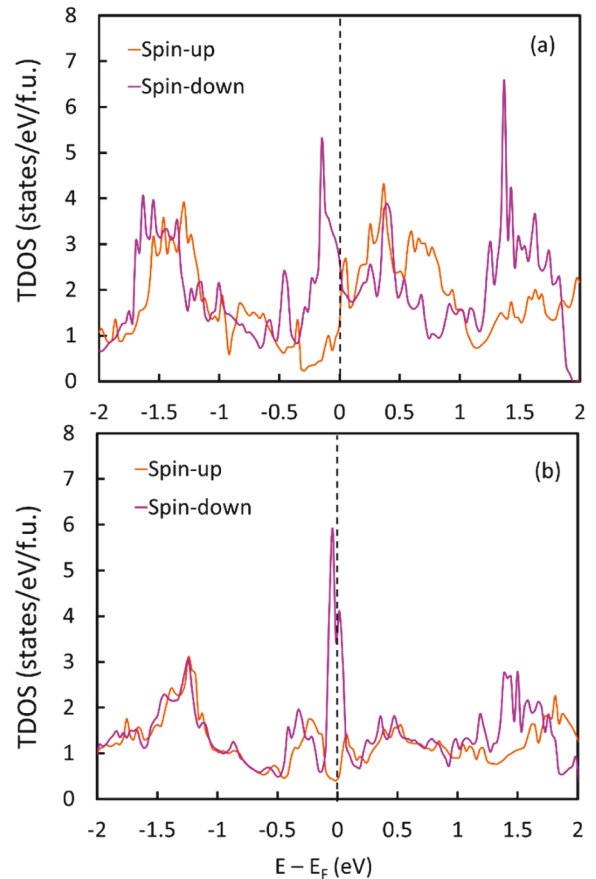magnetic field were previously hypothesized for GdScGeH by Mahon et al. [24], stating that they are a result of weak localization of conduction electrons caused by imperfections, such as Gd/Sc substitutions, hydrogen vacancies, or stacking faults. It is also plausible that a narrow bandgap opening at the Fermi energy, like CeScSiH [23], gives rise to low-temperature non-metallic, Kondo-like behavior. Further examination of the density of states is required to determine the true nature of these materials, see the Electronic-structure section.

Considering the anomalous behavior of the electrical resistivity, we also examined the electronic contribution to the heat capacity of the *PCTPro* hydride. The heat capacity of $Pr_{0.75}Ge_{0.25}ScGeH$ (see Fig. S2, SI) reveals a large nuclear contribution, common in Pr-containing compounds [39], evident from C_P/T upturn at low temperatures. Complex and strong magnetic field dependence of C_P/T at low temperature (initial enhancement in 20 and 50 kOe and suppression in 90 kOe magnetic fields) also indicates additional conventional magnetic contributions. The presence of both makes it impossible to reliably determine the electronic heat capacity coefficient, γ, using standard fitting to the Debye model. Availability of heat capacity data of the isostructural LaScGeH that has Debye temperature, $θ_D = 273$ K, and $γ = 4.9$ mJ/mol K^2 [24], and where only conventional lattice and electronic contributions are present, makes it possible to estimate γ of $Pr_{0.75}Ge_{0.25}ScGeH$, reasonably postulating that $θ_D$ of both are the same (see SI for details). Thus determined $γ = 28.7$ mJ/mol K^2 corresponds to a density of states at the Fermi energy, E_F, of 12.2 states/eV-f.u. (Table 1).

3.3. Electronic-structure calculations

To model the structures of both the $Pr_{0.75}Gd_{0.25}ScGe$ parent and $Pr_{0.75}Gd_{0.25}ScGeH$ hydride, one of the four Pr atoms in a PrScGe unit cell
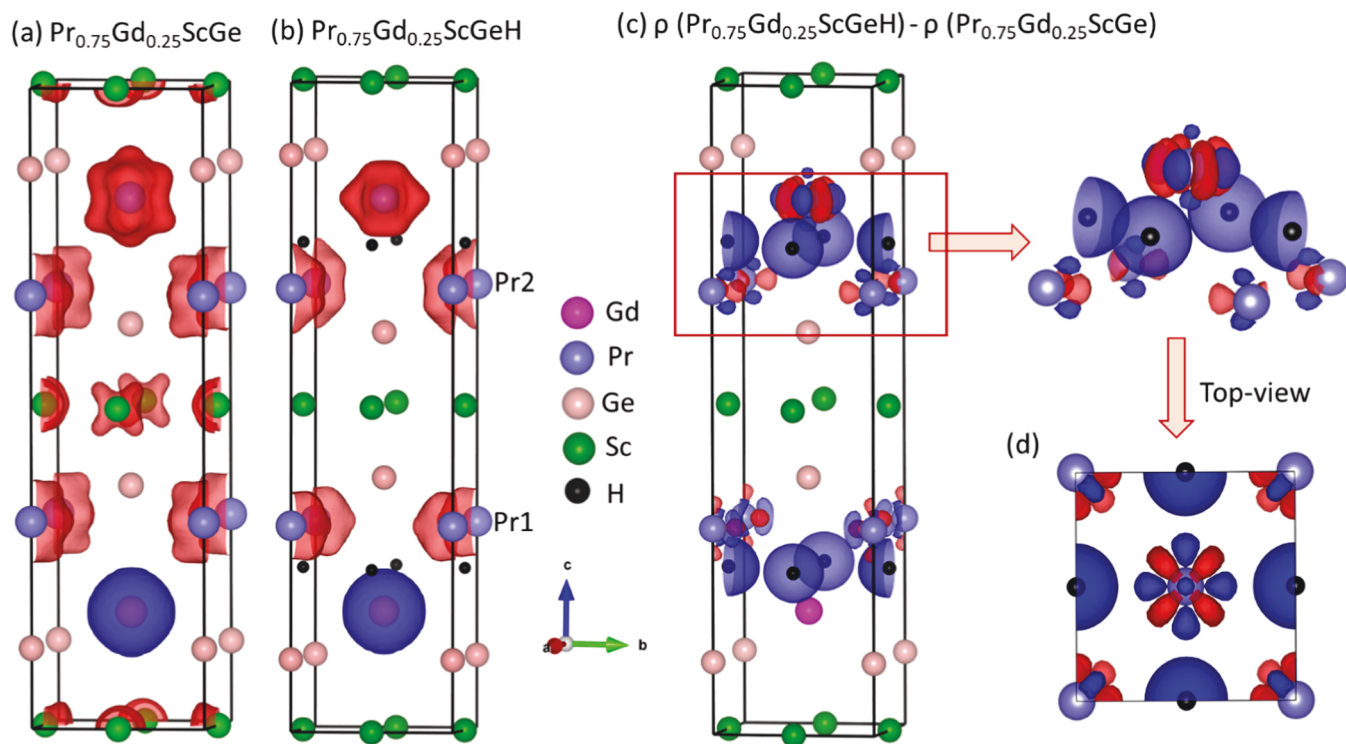
Fig. 6. Spin densities of (a) $Pr_{0.75}Gd_{0.25}ScGe$ and (b) $Pr_{0.75}Gd_{0.25}ScGeH$ shown as $\pm\,0.008$ e/$Å^3$ isosurfaces; positive (spin-up) in blue and negative (spin-down) in red. (c) Total charge-density difference between $Pr_{0.75}Gd_{0.25}ScGe$ and its hydride shown as $\pm\,0.02$ e/$Å^3$ isosurfaces; positive (charge gain) in blue, negative (charge loss) in red. (d) Top view of the fragment highlighted in (c); charge-difference isosurfaces show charge gain (blue) and loss (red). Color-coding of atoms is identical to Fig. 1.

is replaced with Gd after lowering symmetry from the original $I4/mmm$ to $P1$ (Fig. 1a), and the structure is allowed to relax, leading to a reasonable agreement between experiment and theory (Table 1). The Pr atom neighboring the Gd atom is no longer equivalent to the two remaining Pr atoms in the same cell; respectively, these are denoted as Pr1 and Pr2 in Table 1. This simple model represents the "average" unit cell ($Pr_3GdSc_4Ge_4$), not necessarily the case for a given unit cell. Considering a uniform distribution of Pr and Gd atoms in a lattice, the probability that a randomly-selected unit cell contains n Gd atoms ($0 \leq n \leq 4$) is given by $P(n) = \binom{4}{n}0.25^n 0.75^{4-n}$. Thus, there is a 31.6% probability that a unit cell has no Gd atoms ($n = 0$), whereas the corresponding probabilities for n = 1, 2, 3, and 4 are, respectively, 42.2%, 21.1%, 4.7%, and 0.4%; the model of the crystal structure we employ, therefore, represents the most probable case where $n = 1$.

Postulating that magnetic moments of Pr and Gd may be either antiparallel (ferrimagnetic, FiM) or parallel (ferromagnetic, FM), the DFT-derived energy differences $\Delta E = E_{FiM} - E_{FM}$ (Table 1) reveal the stability of FiM at the ground states of both parent and hydride, in agreement with the magnetic property data shown in the physical property section. Hydrogenation increases c, c/a, and unit cell volume. It also reduces the average total Pr-($4f + 5d$) moment from 2.26 μ_B to 2.08 μ_B, whereas the total Gd moment becomes slightly enhanced. The $5d$ moments of Pr (Gd) decrease (increase) with the hydrogenation. Rather significant Sc-$3d$ moments align parallel with those of Pr in the $Pr_{0.75}Gd_{0.25}ScGe$ parent, but they are nearly negligible in the hydride. This reduction of the Pr and Sc moments can be understood from changes in the electronic structure with hydrogen insertion. The partial density of states (PDOS) plotted in Fig. 4 (see Fig. S3, SI, for band structure) reveals strong hybridization of Sc($3d$)-Pr/Gd($5d$) states near E_F in $Pr_{0.75}Gd_{0.25}ScGe$. The spin-polarized Gd/Pr-$5d$ states around the Fermi energy in $Pr_{0.75}Gd_{0.25}ScGe$, are most prominent for Gd, but they diminish with hydrogen insertion, similar to that observed in GdScGe [24]. Likewise, a strong hybridization between Pr/Gd-$5d$ states and

Sc-$3d$ states near E_F is noticeable in $Pr_{0.75}Gd_{0.25}ScGe$, but it also diminishes upon hydrogen insertion. The minority-spin channel of the hydrogenated system (Fig. 4b) has one sharp peak near E_F, contributed by $4f$-states of Pr1-atoms whereas $4f$-states of Pr2 atom are around -3 eV, well below E_F. $4f$ states of Pr1 are hybridized strongly with $5d/3d$-states in the vicinity of E_F in $Pr_{0.75}Gd_{0.25}ScGeH$, unlike in GdScGeH, as populated Gd-$4f$ states are far below E_F. Overall, the insertion of hydrogen into the $Pr_{0.75}Gd_{0.25}ScGe$ lattice reduces both the $5d$-DOS and spin polarization at E_F.

Besides the hybridization of $4f$ and conduction electrons, $5d$-states of lanthanides hybridize with H-$1s$ states around -4 eV, suggesting a chemical bonding between the Ln and H atoms. The Ln-H hybridization, in turn, reduces the $5d$-$3d$ hybridization at E_F, leading to a pseudo-gap in the majority-spin channel (Fig. 5b). The reduced Pr moments and $4f$-conduction electron hybridization near E_F are commensurate with Kondo interactions in the hydrogenated system. Only $4f$-states of Pr1 atoms fall in the vicinity of E_F. Considering that only a third of Pr atoms (Pr1 but not Pr2) contribute to $4f$-conduction electron hybridization and that the reduction of the Pr moment is minor, Kondo interactions in the hydride should be considered weak.

Spin and charge densities of $Pr_{0.75}Gd_{0.25}ScGe$ and its hydride are plotted in Fig. 6. By comparing spin density in the non-hydrogenated and hydrogenated cases, the spin density on the Pr-atoms is clearly reduced in the hydride. The spin density on Sc-atoms that form interlayer "magnetic bridges" between Ln atoms in $Pr_{0.75}Gd_{0.25}ScGe$ vanishes as a result of hydrogenation. Commensurate with the reduced Pr moments and nearly fully diminished Sc moments, these changes in spin density also illustrate how, similar to GdScGeH [24], a 3D magnetic structure of the parent morphs into a quasi-2D structure of the hydride. The charge density difference illustrated in Fig. 6c, demonstrates that hydrogen gains charge and its insertion redistributes mainly the in-plane charge on Pr-atoms, whereas Gd-atoms are practically unaffected. The charge transfer to hydrogen leads to reduced moments on both Pr and Sc
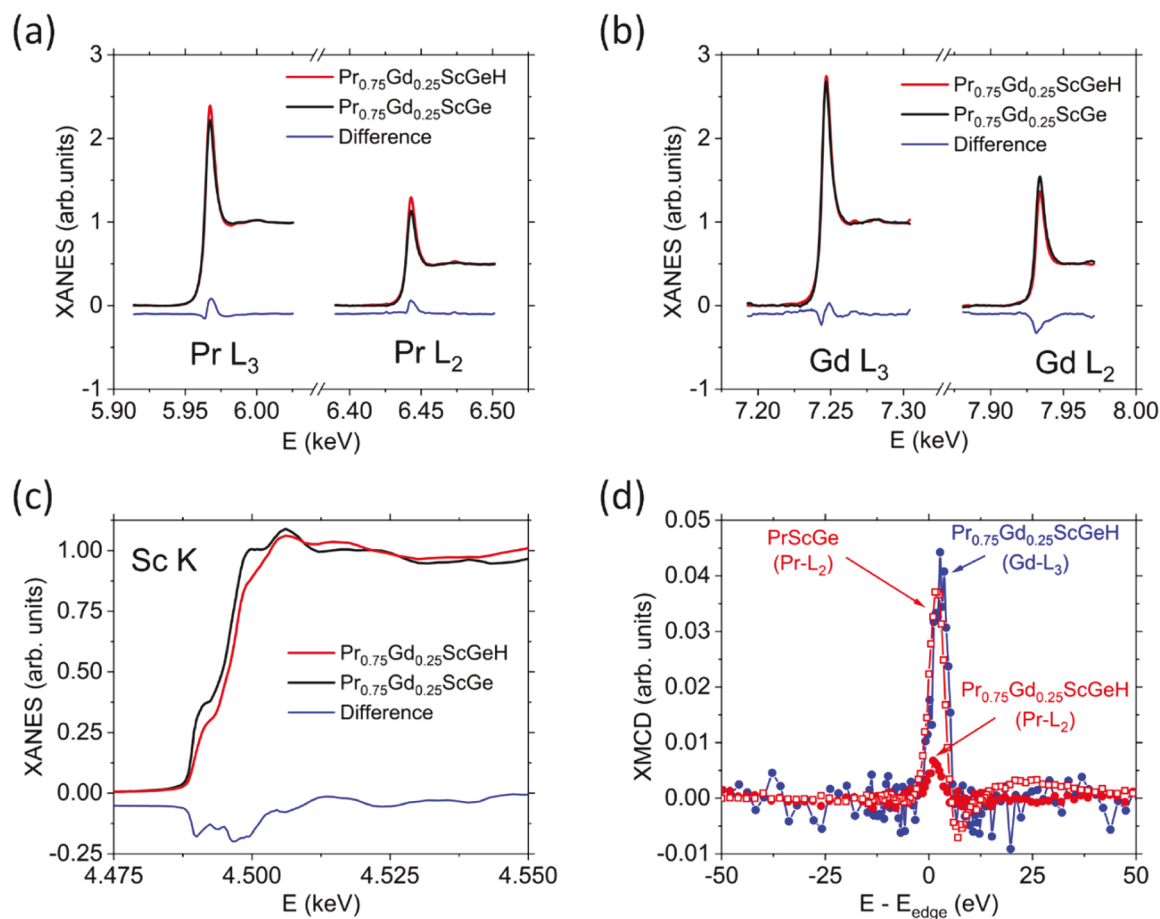
Fig. 7. XANES across the (a) Pr L_2 and L_3, (b) Gd L_2 and Pr L_3, and (c) Sc K edges for $Pr_{0.75}Gd_{0.25}ScGe$ (black) and the *PCTPro* hydride (red). The solid blue lines denote the differences between hydride and parent. XANES of the Gd and Pr edges were performed at 300 K and for the Sc edge at 2 K. (d) XMCD across Pr-L_2 and Gd-L_3 edges of $Pr_{0.75}Gd_{0.25}ScGeH$ and PrScGe obtained at 3 K in 20 kOe applied fields. Positive XMCD is indicative of a projection along the field for both Pr and Gd. E_{edge} is the energy of the respective absorption edges.

atoms and, consequently, to reduced Ln-Sc interactions.

3.4. Spectroscopy

Element-specific XANES spectra for Gd, Pr, and Sc of $Pr_{0.75}Gd_{0.25}ScGe$ and its hydride are depicted in Fig. 7. For Pr and Gd, the measured absorption edges, L_2 and L_3, are for the $2p_{1/2} \rightarrow 5d$ and $2p_{3/2} \rightarrow 5d$ excitations, respectively. The shapes, intensities, and positions of the peaks near the absorption edges can be useful for extracting information about the electronic structure and electronic configurations of the elements [40]. For example, the sum of the L_2 and L_3 "white lines" (large peaks above the threshold) is related to the number of empty $5d$ states above the Fermi energy [40–43].

The L_2 and L_3 white line sum increases (decreases) for Pr (Gd) with hydrogenation. This reveals that the number of empty Pr $5d$ states increases while Gd $5d$ empty states decreases just above the Fermi energy, corroborating the DFT-calculated DOS shown in Fig. 5 (Pr1 $5d$ PDOS drastically increases above E_F, leading to more Pr empty states, while Gd peak directly above E_F disappears with hydrogenation, giving fewer empty states). Additionally, the near-edge structure of Sc changes substantially between the $Pr_{0.75}Gd_{0.25}ScGe$ and the *PCTPro* hydride (Fig. 7c) indicative of large differences in Sc local structure, also in agreement with DFT PDOS calculations (Fig. 4). On the other hand, the stark differences in charge density around Pr between $Pr_{0.75}Gd_{0.25}ScGe$ and the *PCTPro* hydride (Fig. 6) should result in an observable change in the peak shape at the Pr-L_2 and L_3 edges, yet peak shapes of the *PCTPro* hydride are within error of $Pr_{0.75}Gd_{0.25}ScGe$. This difference is likely a result of the difficulties related to proper modeling chemical disorder in DFT in a small unit cell.

XMCD (Fig. 7d) is used to directly probe the coupling of Pr and Gd magnetic sublattices in hydrogenated $Pr_{0.75}Gd_{0.25}ScGe$, and, for reference, PrScGe. As seen, both Pr and Gd sublattices have magnetic moment projections along the applied magnetic field contrary to $Pr_{0.75}Gd_{0.25}ScGe$, where the Pr moment projection opposes the field [29]. Even though XMCD suggests a parallel coupling of Pr and Gd, the signal from the Pr magnetic sublattice (~0.5%) is far weaker than in pure PrScGe (~3.5%) – a material known to be a ferrimagnet with large crystalline electric field effects that reduce Pr moments and, as a result, XMCD signal [44] – as well as its non-hydride parent (~5.0%) [29]. Considering that domains appear at 10 K, it is feasible that the Pr magnetic sublattice is not ordered at 3 K. Hence, the weak XMCD signal indicating that the Pr magnetic projection is along the field is likely a reflection of the *disordered* Pr magnetic sublattice polarized by the *ordered* Gd magnetic sublattice and/or the applied magnetic field. Here we note that the 2 K magnetization as a function of applied magnetic field reaches ~2 μ_B/f.u. (Fig. S4, SI), roughly the expected contribution from the Gd magnetic sublattice, further suggesting that the Pr magnetic sublattice remains disordered at low temperatures. This peculiar magnetic behavior does not conflict with the DFT-calculated magnetic structure as DFT was done at 0 K.

4. Conclusions

We have examined and interpreted the effect of hydrogenation on

crystal structure and physical properties of $Pr_{0.75}Gd_{0.25}ScGe$. The magnetic ordering temperatures of the partially (approximately 0.27 H atoms per formula unit) and fully (1 H atom per formula unit) hydrogenated intermetallic compound are, as seen from AC magnetic susceptibility, 70 K and 10 K, respectively; both are lower than the 190 K magnetic ordering temperature of the non-hydrogenated parent. Experimentally, the Gd and Pr magnetic sublattices in $Pr_{0.75}Gd_{0.25}ScGeH$ order separately, with the Gd magnetic sublattice being ordered and the Pr magnetic sublattice being disordered at 3 K. DFT predicts that at the ground state Gd and Pr order ferrimagnetically.

Like other CeScSi-type structures, hydrogen is inserted into the Ln_4 tetrahedra, contracting the $a(=b)$ lattice parameters, expanding the *c lattice parameter*, and increasing the unit cell volume. Hydrogenation destroys the spin densities on the Sc atoms disconnecting the $Pr_{0.75}Gd_{0.25}$ magnetic layers and forming a quasi-2D magnetic structure. Hybridization of the Gd/Pr 5d states with H 1s states indicate chemical bonding, influencing the magnetic properties of $Pr_{0.75}Gd_{0.25}ScGeH$. The Pr/Gd-H hybridization in the valence band results in weak spin-polarization of conduction electrons at the Fermi energy, E_F, opening a pseudo-gap in the spin-up channel, in contrast to the spin-down channel where E_F is located on a steep slope. Furthermore, hydrogenation causes strong hybridization between the Pr1–4f and 5d/3d-states in the vicinity of E_F, shifting the Pr1–4f states near E_F in the minority channel. The strong 4f hybridization coupled with the pseudo-gap at E_F in the majority-spin channel, suggests hydrogenation induces weak Kondo interactions in the fully hydrogenated $Pr_{0.75}Gd_{0.25}ScGe$ system. Anomalous electrical resistivity behavior stems directly from the competition between weak Kondo interactions and long-range magnetic ordering. Thus, when strong magnetic fields are applied, long-range magnetic ordering dominates, and Kondo behavior is suppressed.

Declaration of Competing Interest

The authors declare the following financial interests/personal relationships which may be considered as potential competing interests: Co-author is lead guest editor for the journal issue - Y.M. Co-author is co-editor for the journal issue - A.K.P.

Data availability

Data will be made available on request.

Acknowledgments

Appendix A. Supporting information

Supplementary data associated with this article can be found in the online version at doi:10.1016/j.jallcom.2023.171351.

References

[1] Y. Tokiwa, M. Garst, P. Gegenwart, S.L. Bud'ko, P.C. Canfield, Quantum bicriticality in the heavy-fermion metamagnet YbAgGe, Phys. Rev. Lett. 111 (2013), 116401.

[2] B. Chevalier, et al., Hydrogenation inducing antiferromagnetism in the heavy-fermion ternary silicide CeRuSi. Phys. Rev. B 77 (2008), 014414.

[3] O. Janka, O. Niehaus, R. Pöttgen, B. Chevalier, Cerium intermetallics with TiNiSi-type structure, Z. fur Naturforsch. B 71 (2016) 737.

[4] S. Gupta, K.G. Suresh, Review on magnetic and related properties of RTX compounds, J. Alloy. Compd. 618 (2015) 562.

[5] R. Pöttgen, B. Chevalier, Cerium intermetallics with ZrNiAl-type structure - A review, Z. fur Naturforsch. B 70 (2015) 289.

[6] F. Bernardini, et al., Iron-based superconductivity extended to the novel silicide LaFeSiH, Phys. Rev. B 97 (2018), 100504.

[7] Z. He, et al., Superconductivity in Co-Layered LaCoSi, Inorg. Chem. 60 (2021) 6157.

[8] R. Pöttgen, D. Johrendt, D. KuBmann, Chapter 207: structure-property relations of ternary equiatomic YbTX intermetallics. Handb. Phys. Chem. Rare Earths 32 (2001) 453.

[9] R. Pöttgen, O. Janka, B. Chevalier, Cerium intermetallics CeTX - Review III. Z. fur Naturforsch. B 71 (2016) 165.

[10] M.A. Ruderman, C. Kittel, Indirect exchange coupling of nuclear magnetic moments by conduction electrons, Phys. Rev. 96 (1954) 99.

[11] T. Kasuya, A Theory of Metallic Ferro-and Antiferromagnetism on Zener's Model, Prog. Theor. Phys. 16 (1956) 45.

[12] K. Yosida, Magnetic properties of Cu-Mn Alloys. Phys. Rev. 106 (1957) 893.

[13] P.G. de Gennes, Interactions indirectes entre couches 4f dans les métaux de terres rares. J. De. Phys. Et. Le. Radium 23 (1962) 510.

[14] J. Kondo, Resistance minimum in dilute magnetic alloys, Prog. Theor. Phys. 32 (1964) 37.

[15] T. Sugawara, Low temperature resistivity of yttrium-based alloys containing small amounts of rare earth metals, J. Phys. Soc. Jpn. 20 (2013) 2252.

[16] J. Boes, A.J. van Dam, J. Bijvoet, Kondo effect in the electrical resistivity of silver-gold alloys with ytterbium. Phys. Lett. A 28 (1968) 101.

[17] K.A. Gschneidner, P. Burgardt, S. Legvold, J. Moorman, 0 & Stassis, C. Kondo scattering in a pure metal- beta cerium: I. Experimental.", J. *Phys. F: Met. Phys.* 6 (1976) L49.

[18] R. Welter, G. Venturini, B. Malaman, Magnetic properties of RFeSi (R=La-Sm, Gd-Dy) from susceptibility measurements and neutron diffraction studies. J. Alloy. Compd. 189 (1992) 49.

[19] B. Chevalier, et al., Magnetic ordering induced by the hydrogenation of the ternary stannide CeNiSn, J. Magn. Magn. Mater. 272 (2004) 576.

[20] O. Isnard, et al., Low-temperature and high-pressure μSR study of the strongly correlated CeNiSn Hx compounds, Phys. Rev. B 93 (2016), 224424.

[21] T.S. Nam, et al., Topological bulk band structures of the hourglass and Dirac nodal-loop types in Ce Kondo systems: CeNiSn, CeRhAs, and CeRhSb. Phys. Rev. B 99 (2019), 125115.

[22] B. Chevalier, et al., Inducing magnetism in the Kondo semiconductor CeRhSb through hydrogenation: antiferromagnetic behavior of the new hydride $CeRhSbH_{0.2}$. Chem. Mater. 19 (2007) 28.

[23] B. Chevalier, et al., New hydrides REScSiH and REScGeH (RE = La, Ce): structure, magnetism, and chemical bonding, Chem. Mater. 22 (2010) 5013.

[24] T. Mahon, et al., Hydrogen insertion in the intermetallic GdScGe: a drastic reduction of the dimensionality of the magnetic and transport properties, Inorg. Chem. 57 (2018) 14230.

[25] E. Gaudin, S.F. Matar, R. Pöttgen, M. Eul, B. Chevalier, Drastic change of the ferromagnetic properties of the ternary germanide GdTiGe through hydrogen insertion. Inorg. Chem. 50 (2011) 11046.

[26] I.A. Tskhadadze, et al., GdTiGe (CeScSi-type structure) and GdTiGe (CeFeSi-type structure) as the coherent phases with different magnetic and hydrogenization properties, Mater. Res. Bull. 34 (10–11) (1999) 1773.

[27] S. Tencé, et al., Hydrogenation studies on NdScSi and NdScGe. J. Solid State Chem. 242 (2016) 168.

[28] T. Del Rose, A.K. Pathak, Y. Mudryk, V.K. Pecharsky, Distinctive exchange bias and unusual memory effects in magnetically compensated $Pr_{0.75}Gd_{0.25}ScGe$. J. Mater. Chem. C 9 (181) (2021).

[29] T.J. Del Rose, Y. Mudryk, D. Haskel, A.K. Pathak, V.K. Pecharsky, Origins of magnetic memory and strong exchange bias bordering magnetic compensation in mixed-lanthanide systems. Phys. Rev. Mater. 044413 (2022).

[30] A.P. Holm, V.K. Pecharsky, K.A. Gschneidner, R. Rink, M.N. Jirmanus, X-ray powder diffractometer for in situ structural studies in magnetic fields from 0 to 35 kOe between 2.2 and 315 K, Rev. Sci. Instrum. 75 (2004) 1081.

[31] B.H. Toby, R.B. von Dreele, GSAS-II: The genesis of a modern open-source all purpose crystallography software package, J. Appl. Crystallogr 46 (2013) 544.

[32] J.C. Lang, G. Srajer, Bragg transmission phase plates for the production of circularly polarized x rays, Rev. Sci. Instrum. 66 (1995) 1540.

[33] G. Kresse, D. Joubert, From ultrasoft pseudopotentials to the projector augmented-wave method, Phys. Rev. B 59 (1999) 1758.

[34] G. Kresse, J. Furthmüller, Efficient iterative schemes for ab initio total-energy calculations using a plane-wave basis set, Phys. Reivew B 54 (1996) 11169.

[35] J.P. Perdew, K. Burke, M. Ernzerhof, Generalized gradient approximation made simple, Phys. Rev. Lett. 77 (1996) 3868.

[36] T. Mahon, S. Tencé, R. Pöttgen, B. Chevalier, E. Gaudin, Study of the structural transition and hydrogenation of CeTiGe. J. Alloy. Compd. 805 (2019) 701.

[37] P. Manfrinetti, M. Pani, A. Palenzona, S.K. Dhar, S. Singh, Single crystal study of the high-Curie-temperature ferromagnet $Gd_{1.02}Sc_{0.98}Ge$ and of $Gd_{2.38}Sc_{2.62}Ge_3$, J. Alloy. Compd. 334 (9) (2002).

[38] A. Biswas, et al., First-order magnetic phase transition in Pr_2In with negligible thermomagnetic hysteresis. Phys. Rev. B 101 (2020), 224402.

[39] A.K. Pathak, D. Paudyal, Y. Mudryk, K.A. Gschneidner, V.K. Pecharsky, Anomalous Schottky specific heat and structural distortion in ferromagnetic $PrAl_2$, Phys. Rev. Lett. 110 (2013), 186405.

[40] J. Röhler, Chapter 71: X-ray absorption and emission spectra. Handb. Phys. Chem. Rare Earths 10 (1987) 453.

[41] A. Fuse, G. Nakamoto, M. Kurisu, N. Ishimatsu, H. Tanida, The valence state of Yb metal under high pressure determined by XANES measurement up to 34.6 GPa. J. Alloy. Compd. 376 (2004) 34.

[42] G. Materlik, J.E. Müller, J.W. Wilkins, L-edge absorption spectra of the rare earths: assessment of the single-particle picture, Phys. Rev. Lett. 50 (1983) 267.

[43] H. Jhans, M. Croft, Systematic trends in the LIII-edge absorption spectra of the rare-earth based systems, J. Magn. Magn. Mater. 47–48 (1985) 203.

[44] P. Manfrinetti, A. v Morozkin, O. Isnard, P. Henry, A. Palenzona, Magnetic structure of the CeScSi-type RScGe compounds (R = Pr, Nd, Tb), J. Alloy. Compd. 450 (2008) 86.